Inorganic Chemistry

Article

pubs.acs.org/IC

High-Temperature Spin Crossover Behavior in a Nitrogen-Rich Fe^{III}-Based System

Cyril Cook,[†] Fatemah Habib,[†] Tomoko Aharen,[†] Rodolphe Clérac,[§,∥] Anguang Hu,[⊥] and Muralee Murugesu*[,†,‡]

[†]Department of Chemistry, University of Ottawa, 10 Marie Curie, Ottawa, ON, K1N6N5, Canada

[‡]Centre for Catalysis Research and Innovation, 30 Marie Curie, Ottawa, ON, K1N6N5, Canada

[§]CNRS, CRPP, UPR 8641, F-33600 Pessac, France

[∥]Univ. Bordeaux, CRPP, UPR 8641, F-33600 Pessac, France

[⊥]Defence Research and Development Canada-Suffield, P.O. Box 4000 Stn Main, Medicine Hat, AB, T1A8K6, Canada

Supporting Information

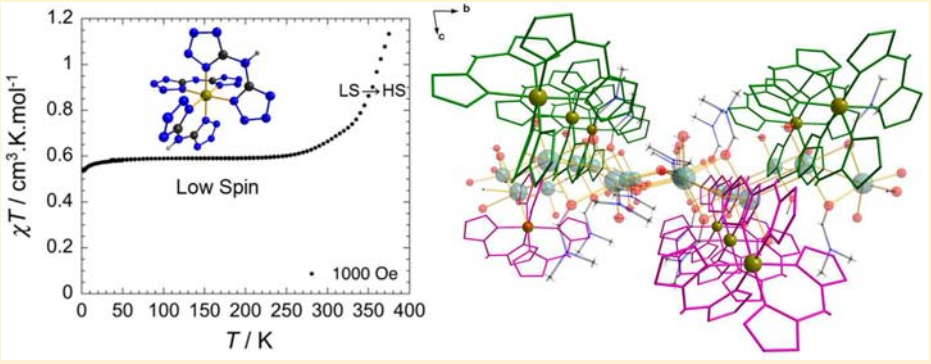

ABSTRACT: A nitrogen-rich ligand *bis*(1*H*-tetrazol-5-yl)amine (H_3bta) was employed to isolate a new Fe^{III} complex, $Na_2NH_4[Fe^{III}(Hbta)_3]\cdot 3DMF\cdot 2H_2O$ (**1**). Single crystal X-ray diffraction revealed that complex **1** consists of Fe^{III} ions in an octahedral environment where each metal ion is coordinated by three $Hbta^{2-}$ ligands forming the $[Fe^{III}(Hbta)_3]^{3-}$ core. Each unit is linked to two one-dimensional (1-D) Na^+/solvent chains creating a two-dimensional (2-D) network. In addition, the presence of multiple hydrogen bonds in all directions between ammonium cation and ligands of different $[Fe^{III}(Hbta)_3]^{3-}$ units generates a three-dimensional (3-D) network. Magnetic measurements confirmed that the Fe^{III} center undergoes a Spin Crossover (SCO) at high temperature ($T_{1/2}$ = 460(10) K).

INTRODUCTION

The design and study of switchable materials have been the focus of significant attention because of potential applications in the field of nanoelectronics.[1,2a] Among the most exciting category of molecular units exhibiting switchable behavior, Spin Crossover (SCO) and Spin Transition (ST) complexes of $3d^4$ to $3d^7$ transition metal ions have been extensively studied for the past decade.[2,3] While the SCO phenomenon consists of a thermal equilibrium (i.e., Boltzmann distribution) between the low spin (LS) ground state and the high spin (HS) state with intermediate-field ligands, ST complexes display a phase transition allowing the system to commute between the two magnetic states with, in some cases, bistable properties (thermal hysteresis effect).[3] It has been well established that these phenomena can be induced by external stimuli such as temperature or pressure variations as well as light irradiation or the application of a magnetic field.[4] The type of LS↔HS phenomenon (SCO vs ST) is controlled by the cooperativity of the material network that is weak and strong for SCO and ST systems, respectively. Such cooperativity is due to the intermolecular elastic interactions, which enable a domino effect spreading the magnetic and structural changes accompanying the LS↔HS conversion. Among all transition metal complexes that exhibit these switchable properties, pure Fe^{III} complexes are less common than other systems.[5,6] Furthermore, only a small portion of these Fe^{III} complexes exhibit a spin-crossover around or above room temperature.[5n−q] Indeed, there are few examples of high-temperature (above 300 K) SCO or ST compounds reported thus far, all of which are *tris*(pyrazol-1-yl)methane, Fe^{II}-based complexes.[7] In addition to the metal center, the ligand plays an important role in the SCO and ST properties. Nitrogen rich (N-rich) chelates are known to act as intermediate-field ligands because of their ability to populate/depopulate d orbitals of higher energy which renders the LS as well as the HS states accessible, a prerequisite for

Received: August 26, 2012
Published: February 6, 2013

   dx.doi.org/10.1021/ic301864d | *Inorg. Chem.* 2013, 52, 1825−1831

SCO or ST complexes. Among N-rich chelates, the *bis*(1*H*-tetrazol-5-yl)amine[8] (H_3bta) ligand, containing two tetrazole rings, has already been used to synthesize some transition metal complexes,[9] including only two Fe^{II} complexes[9h,i] and one using Fe^{III} metal ions.[9j] However, to our knowledge no SCO or ST complex using H_3bta has been reported.

Additionally, N-rich compounds such as those consisting of tetrazole rings can be used as high-energetic materials because of their high N:C ratios. Indeed, with a remarkable 9:2 N:C molar ratio, H_3bta is known to be a potentially energetic ligand and provides high-energy transition metal complexes.[8,9a−c] In addition to its aforementioned properties, H_3bta exhibits multiple deprotonated chelating forms in an acid−base equilibrium (Scheme 1). The two first deprotonated forms,

Scheme 1. Ligand, H_3bta, with All Its Deprotonated Forms

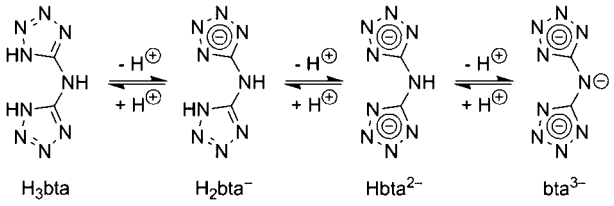

via the deprotonation of each tetrazole ring into the corresponding tetrazolate, are easily accessible because of the possible delocalization of the negative charge through the aromatic tetrazole ring. Although a third deprotonated form can be accessed, the amide anion formation requires more basic conditions. These multiple anionic forms combined with the numerous possible coordination sites through the other nitrogen lone pairs can yield a wide family of coordination complexes: with various metal centers in a variety of oxidation states, different coordination geometries, and multinuclear coordination. Indeed, many types of networks have been observed with different ligand forms, from one-dimensional (1-D) chains[9a−c] to two-dimensional (2-D) and three-dimensional (3-D) networks,[9d−g] with an apparent trend: the more deprotonated the ligand, the higher the dimensionality of the resulting network. Furthermore, a few complexes using the H_3bta ligand have been reported to display interesting catalytic activities toward the combustion of various propellants, accelerating their thermal decomposition with higher decomposition heats.[9b,c]

With this in mind, we have employed the N-rich ligand H_3bta to design a new Fe^{III}-based complex with SCO behavior. Herein we report the synthesis, structural analysis, DFT calculations, and magnetic properties of $Na_2NH_4[Fe^{III}(Hbta)_3]\cdot 3DMF\cdot 2H_2O$ (**1**).

EXPERIMENTAL SECTION

All chemicals and solvents were obtained from commercial sources (Alfa Aesar, Sigma-Aldrich, Fisher Scientific) and were used as received, without further purification.

Caution! *H_3bta in its dehydrated form shows increased friction and impact sensitivity.[8] Although H_3bta·H_2O and complex **1** were kinetically stable, they are nonetheless energetic materials and appropriate safety precautions should be taken, especially when these compounds are prepared on a larger scale. Laboratories and personnel should be properly grounded, and safety equipment such as Kevlar gloves, leather coat, face shield, and earplugs are necessary, especially when manipulating $H_n$bta salts in the dehydrated form.*

Synthesis of Hydrated *bis*(1*H*-tetrazol-5-yl)amine (H_3bta·H_2O). Following a reported procedure,[8,9a] sodium azide (2.60 g, 40 mmol) was added to a white suspension of sodium dicyanamide (1.78 g, 20 mmol) in a mixture of EtOH (30 mL) and water (20 mL). The resulting white suspension, when heated to reflux, became a clear colorless solution. To this refluxing solution was slowly added aq. 2 N HCl (30 mL) dropwise over 1.5 h. After 48 h under reflux, the solution was allowed to cool to room temperature. Concentrated 35% aq. HCl (8 mL) was added dropwise to the clear solution giving a white precipitate which was filtered and washed with water to give H_3bta·H_2O as an amorphous white solid (2.66 g, yield = 79%). The powder X-ray diffraction analysis of the product was in very good agreement with the pattern predicted from the reported X-ray structure of the H_3bta·H_2O (Supporting Information, Figures S1 and S2). Selected IR (cm^{-1}): 3448, 3030, 2948, 2925, 2849, 2667, 2347, 1788, 1641, 1609, 1554, 1458, 1352, 1337, 1282, 1262, 1154, 1109, 1071, 1050, 1036, 1001, 898, 814, 783, 737, 688, 644, 639, 632, 604 (Supporting Information, Figure S3). ^{1}H NMR (methanol-d_4, 300 MHz), δ (ppm) = 4.97 (br s). ^{13}C NMR (methanol-d_4, 75 MHz), δ (ppm) = 155.8.

Synthesis of $Na_2NH_4[Fe^{III}(Hbta)_3]\cdot 3DMF\cdot 2H_2O$ (1). To a colorless solution of the H_3bta·H_2O ligand (152 mg, 0.9 mmol) in a mixture of MeOH (20 mL) and DMF (1.5 mL) was added NaN_3 (39.0 mg, 0.6 mmol) and aq. NH_3 (0.2 mL, 2.7 mmol). After 5 min of stirring at room temperature a solution of $FeCl_2\cdot 4H_2O$ (59.6 mg, 0.3 mmol) in MeOH (3 mL) was added turning the solution deep blue. After another 15 min of stirring, the solution was filtered and placed in a Et_2O diffusion bath. Small dark-blue thin plate crystals of **1** (176.8 mg, yield = 71%) were collected by filtration after 3−4 days. The structure was confirmed by single-crystal X-ray diffraction analysis. Selected IR (cm^{-1}): 3239, 3016, 2895, 2795, 1606, 1544, 1490, 1434, 1324, 1255, 1163, 1116, 1090, 1018, 808, 742, 660 (Supporting Information, Figure S4). ^{1}H NMR (methanol-d_4, 300 MHz), δ (ppm) = 7.97 (s, C*H*O, DMF), 4.88 (br s, H_2O), 4.61 (s, N*H*), 2.98 (s, CH_3, DMF), 2.85 (s, CH_3, DMF). ^{13}C NMR (methanol-d_4, 75 MHz), δ (ppm) = 180.0 (*C*, tetrazole), 164.9 (CHO, DMF), 37.0 (CH_3, DMF), 31.7 (CH_3, DMF). Anal. Calcd for $Na_2NH_4[Fe(Hbta)_3]\cdot 3DMF\cdot 1.5H_2O$ ($C_{15}H_{31}FeN_{31}Na_2O_{4.5}$, MW = 819.44): C, 21.99%; H, 3.81%; N, 52.99%. Found: C, 22.17%; H, 3.94%; N, 53.20%.

Materials and Physical Measurements. Infrared analyses were performed with a Varian 640 FTIR spectrometer equipped with an ATR in the 4000−600 cm^{-1} range. NMR analyses were performed on a Bruker Avance 300 MHz with autotuning broadband probe with Z gradient. Thermo-gravimetric analysis (TGA) data were recorded using an SDT 2960 Simultaneous DSC-TGA instrument at a heating rate of 5 °C/min between 25 and 120 °C, under a constant flow of nitrogen (100 mL/min). Magnetic susceptibility measurements were obtained using a Quantum Design MPMS-XL 7 SQUID magnetometer. The measurements were performed on a polycrystalline sample of **1** (19.26 mg) in a polypropylene bag (3 × 0.5 × 0.02 cm). The dc measurements were conducted in the range of 1.8 to 400 K and between −7 and 7 T applied dc fields. It is worth noting that above 375 K the magnetic susceptibility becomes time dependent indicating a decomposition/evolution of the compound in the magnetometer (under reduced helium pressure; Supporting Information, Figure S17). An *M* vs *H* measurement was performed at 100 K to confirm the absence of ferromagnetic impurities. Experimental data were corrected for the sample holder and for the diamagnetic contribution of the sample.

Single Crystal X-ray Diffraction. Experimental. X-ray crystallographic data for **1** were collected from a single crystal sample mounted on a loop fiber (crystal size: 0.20 × 0.08 × 0.02 mm). Data were collected using a Bruker smart diffractometer equipped with an APEX II CCD Detector, a graphite monochromator (Cu Kα radiation, λ = 1.54178 Å). The crystal-to-detector distance was 5.0 cm, and the data collection was carried out in 512 × 512 pixel mode. The initial unit cell parameters were determined by a least-squares fit of the angular setting of strong reflections, collected by a 10.0 degree scan in 33 frames over four different parts of the reciprocal space (132 frames total). **Geometry:** All esds (except the esd in the dihedral angle between two l.s. planes) are estimated using the full covariance matrix. The cell esds

dx.doi.org/10.1021/ic301864d | *Inorg. Chem.* 2013, 52, 1825−1831

are taken into account individually in the estimation of esds in distances, angles, and torsion angles; correlations between esds in cell parameters are only used when they are defined by crystal symmetry. An approximate (isotropic) treatment of cell esds is used for estimating esds involving l.s. planes. **Refinement:** Refinement of F^2 against ALL reflections. The weighted R-factor wR and goodness of fit S are based on F^2, conventional R-factors R are based on F, with F set to zero for negative F^2. The threshold expression of $F^2 > 2\sigma(F^2)$ is used only for calculating R-factors(gt) and so forth and is not relevant to the choice of reflections for refinement. R-factors based on F^2 are statistically about twice as large as those based on F, and R-factors based on ALL data will be even larger. The data reduction included a correction for Lorentz and polarization effects with an applied multiscan absorption correction (SADABS).[10] The crystal structure was solved and refined using the SHELXTL program suite.[11] Direct methods yielded all non-hydrogen atoms. All hydrogen atom positions were calculated geometrically and were riding on their respective atoms. All non-hydrogen atoms were refined with anisotropic thermal parameters. Crystallographic data for the structure reported in this paper have been deposited with the Cambridge Crystallographic Centre as supplementary publication no. CCDC 894285.

RESULTS AND DISCUSSION

Synthesis. The H_3bta ligand has been synthesized following a known procedure:[8,9a] a [3 + 2] cycloaddition between each cyano group of the sodium dicyanamide and an azide anion under mild acidic condition in a refluxing 3:2 ethanol–water mixture (Scheme 2). After refluxing for 48 h, acidification of the

Scheme 2. Synthesis of Hydrated H_3bta Ligand

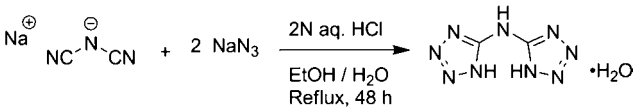

clear solution by addition of concentrated HCl forced the product to precipitate as the hydrated form that appeared as a white solid after filtration. No further purification such as reported treatment with boiling water was necessary since the powder X-ray diffraction analysis supported the purity of the obtained compound, $H_3bta{\cdot}H_2O$.

The iron complex was prepared by adding a solution of $FeCl_2{\cdot}4H_2O$ in methanol to a prestirred solution of $H_3bta{\cdot}H_2O$, NaN_3 and aq. NH_3 in methanol and DMF (7% v/v). Complex **1** was obtained as dark-blue thin plates after 3–4 days of crystallization aided by slow diffusion of Et_2O (Figure 1). The

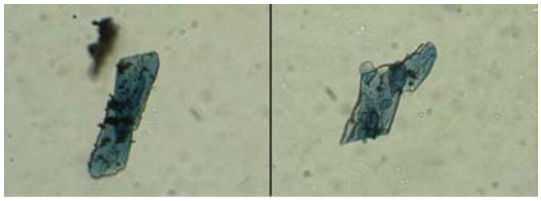

Figure 1. Optical microscopy pictures of complex **1** in the crystalline form showing the dark-blue thin plate crystals. Magnification: microscope ×20; camera ×3.8.

presence of dimethylformamide (DMF) was important to slow the crystallization process to produce crystals suitable for single crystal X-ray diffraction analysis. Additionally, NaN_3 initially used to introduce azide anions as secondary ligands was found to be necessary for crystal growth. Indeed, the Na^+ ions were essential for the isolation of complex **1** as they played a role as counter-cations and allow for **1** to crystallize in a 2-D network arrangement (Supporting Information, Figures S5 and S6). Although Fe^{II} was used as starting material, complex **1** consists of Fe^{III} metal centers, because of the prompt oxidation of Fe^{II} into Fe^{III} under O_2/aqueous conditions. Complex **1** crystallized as small thin plates (Figure 1) and thus growth and isolation of crystals suitable for single-crystal X-ray diffraction were challenging. Furthermore, several attempts to measure X-ray diffraction using a Mo X-ray source did not result in a good diffraction pattern and hence a Cu source was necessary to collect a good data set and be able to solve the structure of **1**. Other reaction conditions were explored using different solvents and base, however, they were fruitless in obtaining complex **1**.

Energetic Properties. As a potential energetic material, complex **1** was subjected to basic preliminary tests to investigate its stability and energetic properties before any other analysis and measurements were performed. Crystals of **1** were first gradually heated up to 250 °C; melting/decomposition was noted around 150 °C with no other behavior being observed. Compound **1** was tested for sensitivity to pressure, friction in a mortar with a pestle, metallic friction between a metallic plate and a spatula, and finally hammering shock test. Ultimately, complex **1** proved to be kinetically stable and insensitive to heat, pressure, friction, and shock. We believe that the lack of energetic properties of **1** is due to the presence of Na^+ counter-cations and solvent molecules within its crystal structure (*vide infra*). By comparison, the ligand itself, H_3bta, is only sensitive to friction and impact in its anhydrous form.[8]

Structural Analysis. Complex **1** crystallizes in the triclinic space group $P\bar{1}$. The crystallographic data for complex **1** are reported in Table 1, and selected bond distances and angles are presented in Table 2. The crystal structure of **1** is presented in Figure 2 (and Supporting Information, Figures S5–S7), with a labeled core structure presented in Figure 3. The core structure consists of an Fe^{III} metal center coordinated by three doubly deprotonated $Hbta^{2-}$ ligands. Each Fe^{III} ion coordinates to six

Table 1. Crystallographic Parameters for Complex 1

formula	$C_{15}H_{32}FeN_{31}Na_2O_5$
MW (g.mol^{-1})	828.55
crystal system	triclinic
space group	$P\bar{1}$
T (K)	100
a (Å)	10.9071(9)
b (Å)	12.8656(10)
c (Å)	13.8554(12)
α (deg)	77.327(4)
β (deg)	71.974(4)
γ (deg)	78.734(4)
V (Å^3)	1786.7(3)
Z	2
wavelength (Å)	1.54178
μ (Cu, Kα), (mm^{-1})	4.313
D_c (g.cm^{-3})	1.540
F (000)	854.0
R_1 ($I > 2\sigma(I)$)[a]	0.1057
wR_2 ($I > 2\sigma(I)$)[b]	0.2967

[a] $R_1 = \sum(||F_o| - |F_c||)/\sum|F_o|$. [b] $wR_2 = [\sum[w(F_o^2 - F_c^2)^2]/\sum[w(F_o^2)^2]]^{1/2}$; $w = 1/[\sigma^2(F_o^2) + (ap)^2 + bp]$, where $p = [\max(F_o^2, 0) + 2F_c^2]/3$, $a = 0.765$, $b = 7.6588$.

dx.doi.org/10.1021/ic301864d | Inorg. Chem. 2013, 52, 1825–1831

Table 2. Selected Distances (Å) and Angles (deg) for 1

		Distances (Å)			
Fe–N(1)	1.952(6)	Fe–N(19)	1.931(6)	Fe···Fe (along *a*)	10.91
Fe–N(9)	1.930(7)	Fe–N(21)	1.948(7)	Fe···Fe (along *b*)	12.87
Fe–N(11)	1.940(7)	Fe–N(29)	1.970(6)	Fe···Fe (along *c*)	8.00
		Angles (deg)			
N(1)–Fe–N(9)	88.3(3)	N(9)–Fe–N(11)	177.4(3)	N(11)–Fe–N(21)	91.5(3)
N(1)–Fe–N(11)	90.5(3)	N(9)–Fe–N(19)	91.0(3)	N(11)–Fe–N(29)	92.2(3)
N(1)–Fe–N(19)	89.4(3)	N(9)–Fe–N(21)	90.9(3)	N(19)–Fe–N(21)	178.0(3)
N(1)–Fe–N(21)	91.0(3)	N(9)–Fe–N(29)	89.1(3)	N(19)–Fe–N(29)	93.1(3)
N(1)–Fe–N(29)	176.4(3)	N(11)–Fe–N(19)	86.6(3)	N(21)–Fe–N(29)	86.6(3)

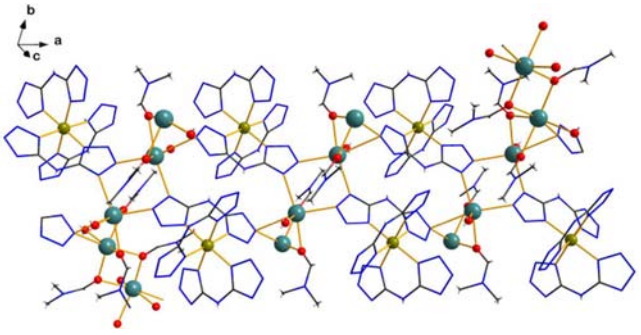

Figure 2. Crystal structure of **1**. Color code: Fe (yellow-green), Na (blue-green), N (blue), C (dark gray), O (red), H (light gray). Ammonium ions are omitted for clarity.

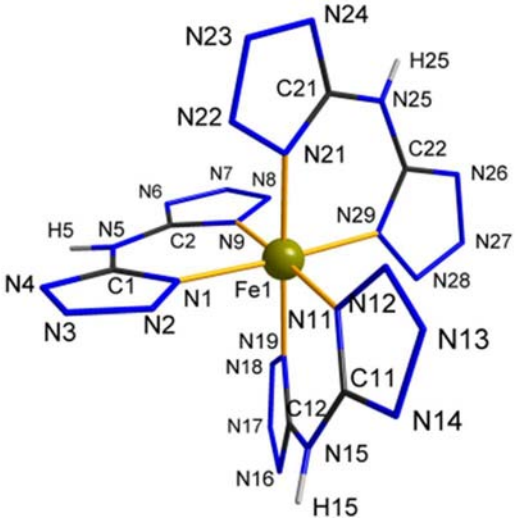

Figure 3. Labeled structural core of **1**. Color code: Fe (yellow-green), N (blue), C (dark gray), H (light gray).

nitrogen atoms in an octahedral environment, and each coordinating N atom belongs to a tetrazole ring from deprotonated $Hbta^{2-}$ ligands. The distances between Fe^{III} and the coordinating N atoms range from 1.930(7)–1.970(6) Å (see Table 2), in agreement with a LS Fe^{III} ion. Indeed, it has been reported that for SCO complexes with Fe^{III} ions in a N_6 octahedral environment, the Fe–N distances in the LS state vary between 1.93 and 2.01 Å, and for the corresponding HS state, the Fe–N distances increase to a 1.97–2.20 Å range.[6] It is noteworthy that SCO complexes with Fe^{III} ions in N_6 octahedral environments[6] represent only few of the Fe^{III} SCO complexes, the majority being in an N_4O_2 octahedral coordination to obtain a suitable ligand field.[5] The opposite applies for Fe^{II} SCO complexes which are usually in N_6 instead of N_4O_2 octahedral environments.

Because of the octahedral coordination environment of the Fe^{III} ions with three bidentate ligands, complex **1** crystallizes as a racemic mixture of the two optical enantiomers Δ and Λ regarding the $[Fe(Hbta)_3]^{3-}$ core (shown in green and pink, respectively, in Figure 4). This phenomenon, discovered by

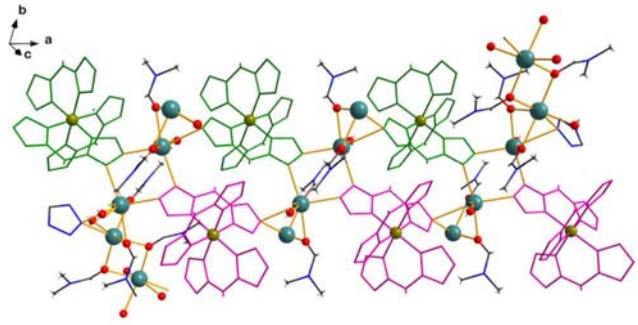

Figure 4. Crystal structure of **1** highlighting the two optical enantiomers Δ (green) and Λ (pink) of the $[Fe(Hbta)_3]^{3-}$ core. Color code: Fe (yellow-green), Na (blue-green), N (blue), C (dark gray), O (red), H (light gray). Ammonium ions are omitted for clarity.

Alfred Werner,[12] occurs in any octahedral *tris*(chelate) complex and is known as coordination-induced chirality. It is noteworthy that molecules sharing the same chirality are aligned along the *a*- and *b*-axes while each enantiomer is only arranged on one side of a pseudo [*ab*] plane constituted by the 1-D Na^+-chains along the *b*-axis (Supporting Information, Figures S8–S9).

Additionally, each $[Fe(Hbta)_3]^{3-}$ core in **1** exhibits interactions with four Na^+ ions through three N atoms from one Hbta ligand molecule. Interactions take place between N13···Na1 (2.863 Å), N13···Na2 (2.536 Å), N16···Na1 (2.547 Å), N17···Na1 (2.474 Å) (Supporting Information, Figure S10). The Na^+ ions are also in an octahedral coordination environment: Na1 is in a N_3O_3 octahedral environment with three N atoms (N13, N16, and N17) from three ligand molecules, and three O atoms from a water molecule and two DMF molecules; Na2 is in a NO_5 octahedral environment with N13 and five O atoms from a water molecule and four DMF molecules. Analysis of the packing diagram of **1** shows that all the Na^+ ions exhibit a -Na1-Na1-Na2-Na2-Na1-Na1- zigzag 1-D chain along the *b*-axis (Supporting Information, Figure S11). The Na^+ ions are linked in the chain through nitrogen atoms from multiple $[Fe(Hbta)_3]^{3-}$ units, and oxygen atoms from DMF molecules (Supporting Information, Figures S10–S11).

In addition, every $[Fe(Hbta)_3]^{3-}$ unit interacts along the *a*-axis with two distinct Na^+ chains. The multiple N···Na interactions along the *a*-axis linked to the Na^+ 1-D chain

dx.doi.org/10.1021/ic301864d | *Inorg. Chem.* 2013, 52, 1825–1831

along the *b*-axis create a 2-D network along the [*ab*] plane with moderately buffered connectivity due to the solvent molecules within the Na^+ 1-D chain. Besides, one can notice the presence of multiple hydrogen bonds (Supporting Information, Table S1, Figure S12) between the NH and a N atom from the tetrazolate ring of two ligands of two different $[Fe(Hbta)_3]^{3-}$ units (N5−H5···N6, N15−H15···N2, and N25−H25···N24), and between ammonium ion and four N atoms from the tetrazolate rings of four Hbta ligands of four different $[Fe(Hbta)_3]^{3-}$ units (N61−H61a···N26, N61−H61b···N7, N61−H61c···N4, and N61−H61d···N23). The H···N and N···N distances are in a range of 1.98−2.16 Å and 2.800(8)−2.968(10) Å respectively, in good agreement with observed N−H···N hydrogen bonds.[13] The N−H···N angles range from 149.9° to 151.1°. The presence of these multiple hydrogen bonds between ligand/ligand and between ligand/ammonium ions generates a 3-D network of weak interactions. The shortest inter-unit Fe···Fe distances are 10.91, 12.87, and 8.00 Å along the *a*-, *b*-, and *c*-axes, respectively. The short Fe···Fe distance of 8.00 Å along the *c*-axis can be explained by the presence of off-center parallel $\pi-\pi$ stacking interactions along the *b*-axis between the aromatic tetrazole rings of two Hbta ligands from two different $[Fe(Hbta)_3]^{3-}$ units with a distance of 4.84 Å between the two ring centroids, in addition to the N15−H15···N2 hydrogen bonds with a H15···N2 distance of 2.16 Å (Supporting Information, Figure S13). The 3-D network connectivity as well as short intermolecular distances, especially along the *c*-axis representing the interlayer distance, both point toward potential cooperativity in the system between potentially SCO $[Fe(Hbta)_3]^{3-}$ complexes.

The TGA of **1** measured between 25 and 120 °C displays two steps in the weight loss process (Supporting Information, Figure S14). The first step takes place between 30 and 65 °C with an inflection point at 54.2 °C and represents a loss of about 4.5% of the total weight. This is in good agreement with the theoretical value of 4.35% of the total weight corresponding to the loss of the two molecules of water from the crystal structure of **1**. The second step displays a significant weight loss between 65 and 80 °C with an inflection point at 72.3 °C followed by a gradual loss up to 120 °C. The loss between 65 and 120 °C represents approximately 5% of the total weight which is less than the theoretical value of 8.82% of the total weight corresponding to the loss of one of the three molecules of DMF. We can assume that from 25 to 120 °C, **1** loses its two molecules of water and most likely one molecule of DMF. The loss of these coordinated solvent molecules may have an important impact on the crystal structure of **1** regarding the magnetic measurements at high temperature (*vide infra*).

First-Principles Simulations - DFT Calculations. Based on the crystallographic information for the structure of **1**, first-principles simulations were performed within the context of density functional theory (DFT) using the Perdew-Burke-Ernzerhof exchange-correlation functional[14] as implemented in the SIESTA package.[15] The Troullier-Martin norm-conserving pseudopotentials[16] were utilized with nitrogen and carbon reference configurations of $[He]2s^22p^3$ and $[He]2s^22p^2$, along costumed SIESTA basis sets of numerical double-ζ and polarization auxiliary basis functions. The cutoff radii of pseudopotentials are 1.25, 1.25, 1.25, 1.14, 2.38, and 2.41 Å for hydrogen, carbon, nitrogen, oxygen, sodium, and iron, respectively. A 20.0 Å cutoff was employed for the k-point sampling in total energy minimization calculations using the conjugate gradient method without any constraint on symmetry. In the simulations, atomic positions were optimized with the magnitude of forces on each atom smaller than 0.005 eV/Å. Supporting Information, Figure S15 shows the second-order radial distribution function for the crystal structure factor of **1** in comparison with the experimental crystal structure factor. The band structure calculated with the simulated crystal structure shows that **1** is an insulator with about 3.39 eV of energy gap (Supporting Information, Figure S16). The calculated electron density difference contour (Figure 5),

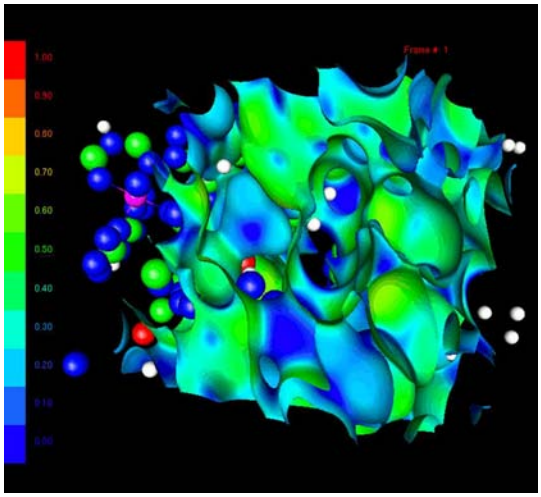

Figure 5. Electron density mapping onto electron density difference against neutral atomic density, generated from the equation $\delta\rho(\vec{r}) = \rho(\vec{r}) - \rho_{atoms}(\vec{r})$ where $\rho(\vec{r})$ is the electron density and $\rho_{atoms}(\vec{r})$ is the neutral atom electron density. Color code: Fe (pink), Na (gray), N (blue), C (green), O (red), H (white).

generated from the equation $\delta\rho(\vec{r}) = \rho(\vec{r}) - \rho_{atoms}(\vec{r})$ where $\rho(\vec{r})$ is the electron density and $\rho_{atoms}(\vec{r})$ is the neutral atom electron density, shows strong electron density depletion around metal sites. This indicates a strong electron delocalization around the Fe sites, which may have effects on the magnetic susceptibility because of electron superexchange interactions.

Magnetic Properties. Magnetic susceptibility measurements have been performed on a polycrystalline sample of **1** (Figure 6). At 1.8 K the χT product is equal to 0.53 cm^3 K mol^{-1} and then slowly increases to a plateau at 0.58 cm^3 K mol^{-1} between 50 and 250 K. This low temperature magnetic behavior is typical of an $S = 1/2$ Fe^{III} low spin species with a significant orbital contribution that enhanced the *g* factor to approximately 2.49 as usually observed in such systems.[2e,17] Above 250 K, the χT product increases significantly to reach 1.15 cm^3 K mol^{-1} at 375 K.

This thermal behavior is typical of a SCO behavior involving the $S = 1/2$ ground state and the thermally populated $S = 5/2$ excited state of an Fe^{III} metal ion complex.[5,6] Unfortunately, the magnetic susceptibility data of **1** becomes irreversible if the compound is heated above 375 K (Supporting Information, Figure S17) and thus the full SCO process cannot be observed. It is worth noting that no significant thermal hysteresis or irreversibility was observed when the temperature is cycled below 375 K even if water and DMF molecules are removed from the solid during the first heating of the sample in the SQUID magnetometer based on the TGA data (*vide supra*). Modeling the χT vs *T* data of **1** using the ideal solution model[18] produced a best fit with the following parameters: ΔH =

dx.doi.org/10.1021/ic301864d | Inorg. Chem. 2013, 52, 1825−1831

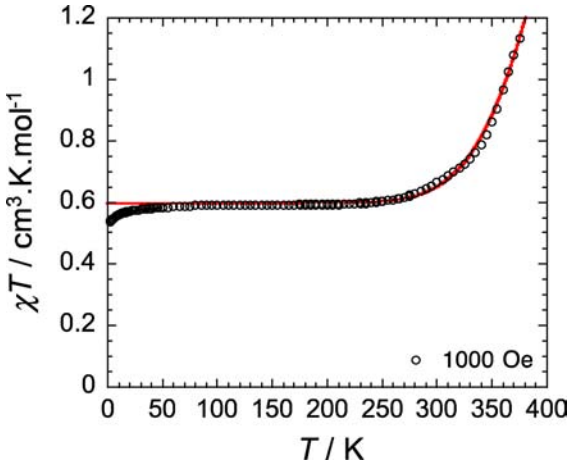

Figure 6. Temperature dependence of the χT product (χ is the molar magnetic susceptibility that is equal to M/H per Fe^{III} complex) at 1000 Oe for **1**. The solid line is the best fit of the data above 150 K with the SCO ideal solution model described in the text.[18]

30.7(9) kJ/mol, $T_{1/2}$ = 460(10) K and thus ΔS = 66(1) J/K/mol (solid line in Figure 6, it is worth noting that χT_{LS} and χT_{HS} have been fixed to 0.58 and 4.375 cm^3 K mol^{-1}, respectively to get a unique solution to the fitting procedure). These enthalpic and entropic thermodynamic parameters are quite reasonable when compared with those previously reported for Fe^{III} spin crossover complexes.[19] As often observed, the entropy change associated with the SCO process, ΔS, is greater than the electronic spin change expected for an Fe^{III}ion, $\Delta S_{spin} = R \ln[(2S_{HS} + 1)/(2S_{LS} + 1)]$ = 9.13 J/K/mol. The remaining entropy variation, approximately 57 J/K/mol, is mainly attributed to nonelectronic vibrations.[20] Even if the crystal structure analysis is clearly showing weak interactions between $[Fe(Hbta)_3]^{3-}$ units (*vide supra*), these elastic couplings are not sufficient to promote strong cooperativity and a spin transition in **1**.

The M vs H data for **1** at low temperatures reveals a close saturation of the magnetization (Supporting Information, Figure S17) at 7 T and 1.8 K. The magnetization reaches a maximum value of 1.21 μ_B at 1.83 K and 7 T that is close to the expected value of 1.25 μ_B for an S = 1/2 system and g = 2.49. The magnetization data plotted as M vs HT^{-1} (Supporting Information, Figure S18) show a quasi-superposition of the measurements between 1.83 and 8 K for dc field up to 7 T, suggesting a weak or negligible magnetic anisotropy and/or the absence of low lying excited states. These data can be well fitted to an S = 1/2 Brillouin function with a g factor of 2.40(5) (Supporting Information, Figure S19).

The magnetic susceptibility and magnetization data confirm without ambiguity the Fe^{III} SCO behavior in complex **1** between an S = 1/2 low spin ground state and a thermally populated S = 5/2 high spin state.

CONCLUSION

A novel Fe^{III} complex using the N-rich ligand H_3bta (*bis*(1*H*-tetrazol-5-yl)amine) was synthesized and thoroughly studied. Complex **1**, $Na_2NH_4[Fe^{III}(Hbta)_3]\cdot 3DMF\cdot 2H_2O$, displays a central core consisting of an Fe^{III} ion in an octahedral coordination environment formed by three bidentate $Hbta^{2-}$ ligands. The $[Fe^{III}(Hbta)_3]^{3-}$ cores interact with a 1-D chain of Na^+/solvent molecules to create a 2-D network. These layers are further connected to a 3-D network through N−H···N hydrogen bonding in all directions between two separate $Hbta^{2-}$ ligand molecules and between ammonium ion and four separate $Hbta^{2-}$ ligand molecules. DFT calculation revealed that complex **1** is an insulator with an energy gap of approximately 3.39 eV and displays strong electron density depletion around the metal sites. Magnetic studies indicated that complex **1** exhibits SCO behavior at high temperature, above 300 K ($T_{1/2}$ = 460(10) K), which makes complex **1** one of the rare Fe^{III} SCO complexes with a high temperature spin-crossover. Unfortunately, the degradation of **1** at higher temperature (above 375 K) did not allow the observation of a complete LS↔HS crossover by the magnetic measurements as well as the structural analysis. Further experiments are currently being carried out to slightly modify the existing system and fine-tune the complex structure around the $[Fe^{III}(Hbta)_3]$ core. This may result in higher temperature stability of the complex and/or a decrease in the $T_{1/2}$ temperature, and thus allow for the study of the complete LS↔HS crossover.

ASSOCIATED CONTENT

Supporting Information

Powder X-ray diffraction pattern of ligand H_3bta (Figures S1−S2), IR spectra of ligand H_3bta and complex **1** (Figures S3−S4), packing arrangement figures of **1** (Figures S5−S11), TGA plot for **1** (Figure S12), simulated second-order radial distribution function plot of **1** (Figure S13), band structure plot of **1** (Figure S14), and additional magnetic data of **1** (Figures S15−S17). X-ray crystallographic information file (CIF) for the structure of complex **1** (deposited at the CCDC with deposition number 894285). This material is available free of charge via the Internet at http://pubs.acs.org.

AUTHOR INFORMATION

Corresponding Author

*E-mail: m.murugesu@uottawa.ca. Fax: +1 (613) 562 5170. Tel: +1 (613) 562 5800 ext. 2733.

Notes

The authors declare no competing financial interest.

ACKNOWLEDGMENTS

This project was solely funded by Defence Research and Development Canada. We thank Françine Bélanger from the X-ray diffraction laboratory at University of Montreal who solved and refined the structure of complex **1**, as well as the CNRS, the University of Bordeaux, and the Conseil Régional d'Aquitaine.

REFERENCES

(1) (a) Kahn, O.; Martinez, C. J. *Science* **1998**, *279*, 44. (b) Kahn, O.; Kröber, J.; Jay, C. *Adv. Mater.* **1992**, *4*, 718. (c) Muller, R. N.; Elst, L. V.; Laurent, S. *J. Am. Chem. Soc.* **2003**, *125*, 8405. (d) Galet, A.; Gaspar, A. B.; Muñoz, M. C.; Bukin, G. V.; Levchenko, G.; Real, J. A. *Adv. Mater.* **2005**, *17*, 2949. (e) Venkataramani, S.; Jana, U.; Dommaschk, M.; Sönnichsen, F. D.; Tuczek, F.; Herges, R. *Science* **2011**, *331*, 445. (f) Larionova, J.; Salmon, L.; Guari, Y.; Tokarev, A.; Molvinger, K.; Molnár, G.; Bousseksou, A. *Angew. Chem., Int. Ed.* **2008**, *47*, 8236.

(2) (a) Gütlich, P.; Garcia, Y.; Goodwin, H. A. *Chem. Soc. Rev.* **2000**, *29*, 419. (b) Gütlich, P.; Garcia, Y.; Woike, T. *Coord. Chem. Rev.* **2001**, *219*, 839. (c) Gaspar, A. B.; Seredyuk, M.; Gütlich, P. *J. Mol. Struct.* **2009**, *924*, 9. (d) Brooker, S.; Kitchen, J. A. *Dalton Trans.* **2009**, 7331. (e) Kahn, O. *Molecular Magnetism*; VCH Publishers: New York, 1993; (f) Djukic, B.; Poddutoori, P. K.; Dube, P. A.; Seda, T.; Jenkins, H. A.;

Lemaire, M. T. *Inorg. Chem.* **2009**, *48*, 6109. (g) Madhu, N. T.; Salitros, I.; Schramm, F.; Klyatskaya, S.; Fuhr, O.; Ruben, M. *C. R. Chim.* **2008**, *11*, 1166. (h) Shuvaev, K. V.; Dawe, L. N.; Thompson, L. K. *Dalton Trans.* **2010**, *39*, 4768. (i) Zhang, L.; Xu, G.-C.; Xu, H.-B.; Mereacre, V.; Wang, Z.-M.; Powell, A. K.; Gao, S. *Dalton Trans.* **2010**, *39*, 4856. (j) Kitchen, J. A.; Jameson, G. N. L.; Tallon, J. L.; Brooker, S. *Chem. Commun.* **2010**, *46*, 3200. (k) Murray, K. S.; Kepert, C. J. *Top. Curr. Chem.* **2004**, *233*, 195.

(3) Gütlich, P.; Goodwin, H. A. *Spin Crossover in Transition Metal Compounds*; Springer: Berlin, Germany, 2004.

(4) (a) Real, J. A.; Gaspar, A. B.; Niel, V.; Muñoz, M. C. *Coord. Chem. Rev.* **2003**, *236*, 121. (b) Real, J. A.; Gaspar, A. B.; Muñoz, M. C. *Dalton Trans.* **2005**, 2062. (c) Gütlich, P.; Hauser, A.; Spiering, H. *Angew. Chem.* **1994**, *106*, 2109; *Angew. Chem., Int. Ed. Engl.* **1994**, *33*, 2024.

(5) (a) Bannwarth, A.; Schmidt, S. O.; Peters, G.; Soennichsen, F. D.; Thimm, W.; Herges, R.; Tuczek, F. *Eur. J. Inorg. Chem.* **2012**, 2776. (b) Fujinami, T.; Nishi, K.; Kitashima, R.; Murakami, K.; Matsumoto, N.; Iijima, S.; Toriumi, K. *Inorg. Chim. Acta* **2011**, *376*, 136. (c) Shimizu, T.; Komatsu, Y.; Kamihata, H.; Lee, Y. H.; Fuyuhiro, A.; Iijima, S.; Hayami, S. *J. Inclusion Phenom. Macrocyclic Chem.* **2011**, *71*, 363. (d) Ortega-Villar, N. A.; Munoz, M. C.; Real, J. A. *Eur. J. Inorg. Chem.* **2010**, 5563. (e) Martinho, P. N.; Harding, C. J.; Mueller-Bunz, H.; Albrecht, M.; Morgan, G. G. *Eur. J. Inorg. Chem.* **2010**, 675. (f) Ross, T. M.; Neville, S. M.; Innes, D. S.; Turner, D. R.; Moubaraki, B.; Murray, K. S. *Dalton Trans.* **2010**, 149. (g) Collet, E.; Boillot, M. L.; Hebert, J.; Moisan, N.; Servol, M.; Lorenc, M.; Toupet, L.; Buron-Le Cointe, M.; Tissot, A.; Sainton, J. *Acta Crystallogr.* **2009**, *B65*, 474. (h) Nemec, I.; Boca, R.; Herchel, R.; Travnicek, Z.; Gembicky, M.; Linert, W. *Monatsh. Chem.* **2009**, *140*, 815. (i) Imatomi, S.; Hashimoto, S.; Matsumoto, N. *Eur. J. Inorg. Chem.* **2009**, 721. (j) Weber, B.; Jäger, E.-G. *Eur. J. Inorg. Chem.* **2009**, 465. (k) Imatomi, S.; Sato, T.; Hamamatsu, T.; Kitashima, R.; Matsumoto, N. *Bull. Chem. Soc. Jpn.* **2007**, *80*, 2375. (l) Masayuki, N.; Takuya, S.; Maeda, Y.; Oshio, H. *Coord. Chem. Rev.* **2007**, *251*, 2606. (m) van Koningsbruggen, P. J.; Maeda, Y.; Oshio, H. *Top. Curr. Chem.* **2004**, *233*, 259. (n) Shongwe, M. S.; Al-Rahbi, S. H.; Al-Azani, M. A.; Al-Muharbi, A. A.; Al-Mjeni, F.; Matoga, D.; Gismelseed, A.; Al-Omari, I. A.; Yousif, A.; Adams, H.; Morris, M. J.; Mikuriya, M. *Dalton Trans.* **2012**, *41*, 2500. (o) Yemeli Tido, E. W.; van Ekenstein, G. O. R. A.; Meetsma, A.; van Koningsbruggen, P. J. *Inorg. Chem.* **2008**, *47*, 143. (p) Juhász, G.; Hayami, S.; Sato, O.; Maeda, Y. *Chem. Phys. Lett.* **2002**, *364*, 164. (q) Hayami, S.; Gu, Z.; Yoshiki, H.; Fujishima, A.; Sato, O. *J. Am. Chem. Soc.* **2001**, *123*, 11644.

(6) (a) Sunatsuki, Y.; Ikuta, Y.; Matsumoto, N.; Ohta, H.; Kojima, M.; Hayami, S.; Maeda, Y.; Kaizaki, S.; Dahan, F.; Tuchagues, J.-P. *Angew. Chem., Int. Ed.* **2003**, *42*, 1614. (b) Ohta, H.; Sunatsuki, Y.; Kojima, M.; Iijima, S.; Akashi, H.; Matsumoto, N. *Chem. Lett.* **2004**, *33*, 350. (c) Sunatsuki, Y.; Ohta, H.; Kojima, M.; Ikuta, Y.; Goto, Y.; Matsumoto, N.; Iijima, S.; Akashi, H.; Kaizaki, S.; Dahan, F.; Tuchagues, J.-P. *Inorg. Chem.* **2004**, *43*, 4154. (d) Brewer, C.; Brewer, G.; Butcher, R. J.; Carpenter, E. E.; Cuenca, L.; Noll, B. C.; Scheidt, W. R.; Viragh, C.; Zavalij, P. Y.; Zielaski, D. *Dalton Trans.* **2006**, 1009.

(7) (a) Schneider, C. J.; Moubaraki, B.; Cashion, J. D.; Turner, D. R.; Leita, B. A.; Batten, S. R.; Murray, K. S. *Dalton Trans.* **2011**, *40*, 6939. (b) Shakirova, O. G.; Lavrenova, L. G.; Naumov, D. Y.; Daletsky, V. A.; Sheludyakova, L. A. *Polyhedron* **2012**, *31*, 64. (c) Shakirova, O. G.; Lavrenova, L. G.; Daletsky, V. A.; Shusharina, E. A.; Griaznova, T. P.; Katsyuba, S. A.; Syakaev, V. V.; Skripacheva, V. V.; Mustafina, A. R.; Solovieva, S. E. *Inorg. Chim. Acta* **2010**, *363*, 4059.

(8) Klapötke, T. M.; Mayer, P.; Stierstorfer, J.; Weigand, J. J. *J. Mater. Chem.* **2008**, *18*, 5248.

(9) (a) Friedrich, M.; Gálvez-Ruiz, J. C.; Klapötke, T. M.; Mayer, P.; Weber, B.; Weigand, J. J. *Inorg. Chem.* **2005**, *44*, 8044. (b) Xue, B.-D.; Yang, Q.; Chen, S.-P.; Gao, S.-L. *J. Therm. Anal. Calorim.* **2010**, *101*, 997. (c) Wang, W.; Chen, S.; Gao, S. *Eur. J. Inorg. Chem.* **2009**, 3475. (d) Zheng, L.-L.; Li, H.-X.; Leng, J.-D.; Wang, J.; Tong, M.-L. *Eur. J. Inorg. Chem.* **2008**, 213. (e) Lu, Y.-B.; Wang, M.-S.; Zhou, W.-W.; Xu, G.; Guo, G.-C.; Huang, J.-S. *Inorg. Chem.* **2008**, *47*, 8935. (f) Jiang, T.; Zhang, X.-M. *Cryst. Growth Des.* **2008**, *8*, 3077. (g) Lin, J.-M.; Huang, B.-S.; Guan, Y.-F.; Liu, Z.-Q.; Wang, D.-Y.; Dong, W. *CrystEngComm* **2009**, *11*, 329. (h) Guan, Y.-F.; Zhou, A.-J.; Wang, D.-Y.; Wang, J.; Dong, W. *J. Mol. Struct.* **2009**, *938*, 150. (i) Guan, Y.-F.; Wang, D.-Y.; Dong, W. *Acta Crystallogr.* **2007**, *E63*, m3150. (j) Only one patent claims the synthesis of an ammonium complex with a $[Fe^{III}(Hbta)_3]^-$ core but without any crystal structure reported: Tappan, B. C.; Huynh, M. H. V.; Hiskey, M. A.; Son, S. F.; Oschwald, D. M.; Chavez, D. E. U.S. Patent Appl. Publ., US 2006/0078454 A1, 2006. (k) Gao, E.-Q.; Liu, N.; Cheng, A.-L.; Gao, S. *Chem. Commun.* **2007**, 2470.

(10) *SADABS, Bruker Area Detector Absorption Corrections*; Bruker Analytical X-ray Systems Inc.: Madison, WI.

(11) (a) *SHELXTL*, v. 6.12; Bruker Analytical X-ray Systems Inc.: Madison, WI, 2001. (b) Sheldrick, G. M. *Acta Crystallogr.* **2008**, *A64*, 112.

(12) (a) Werner, A. *Chem. Ber.* **1911**, *44*, 1887. (b) Werner, A. *Chem. Ber.* **1913**, *46*, 3674. (c) Werner, A. *Chem. Ber.* **1914**, *47*, 3087.

(13) (a) Wallwork, S. C. *Acta Crystallogr.* **1962**, *15*, 758. (b) Steiner, T. *J. Chem. Soc., Chem. Commun.* **1995**, 1331.

(14) Perdew, J. P.; Burke, K.; Ernzerhof, M. *Phys. Rev. Lett.* **1996**, *77*, 3865.

(15) Soler, J. M.; Artacho, E.; Gale, J. D.; García, A.; Junquera, J.; Ordejón, P.; Sánchez-Portal, D. *J. Phys.: Condens. Matter* **2002**, *14*, 2745.

(16) Troullier, N.; Martins, J. L. *Phys. Rev. B* **1991**, *43*, 1993.

(17) Tang, J.; Sanchez Costa, J.; Smulders, S.; Molnar, G.; Bousseksou, A.; Teat, S. J.; Li, Y.; van Albada, G. A.; Gamez, P.; Reedijk, J. *Inorg. Chem.* **2009**, *48*, 2128.

(18) (a) Atkins, P.; De. Paula, J. *Physical Chemistry*, 8th ed.; Oxford University Press: New York, 2006; Chapter 5. (b) Kahn, O. *Molecular Magnetism*; VCH: New York, 1993; p 60. Note that $T_{1/2}$ is defined as the temperature for which the material contains equal quantities of HS and LS species.

(19) Sorai, M.; Nagano, Y.; Conti, A. J.; Hendrickson, D. N. *J. Phys. Chem. Solids* **1994**, *55*, 317. Ortega-Villar, N.; Munoz, M. C.; Real, J. A. *Eur. J. Inorg. Chem.* **2010**, 6653.

(20) Sorai, M. *Chem. Rev.* **2006**, *106*, 976.